MOLECULAR SIMULATION FOR PREDICTING MECHANICAL STRENGTH OF 3-D JUNCTIONED CARBON NANOSTRUCTURES

S. Sihn[a,b*], V. Varshney[a,c], A. K. Roy[a], B. L. Farmer[a]

[a]*Air Force Research Laboratory, AFRL/RXAN, Wright-Patterson AFB, OH 45433, USA*
[b]*University of Dayton Research Institute, Dayton, OH 45469-0060, USA*
[c]*Universal Technology Corporation, Dayton, OH 45432, USA*
**sangwook@alumni.stanford.edu*

Keywords: Molecular model, Strength, Carbon nanotube, Graphene.

Abstract
We have developed a computational scheme to predict stiffness and strength of carbon nanostructures under various loading modes. The prediction method is based on combined molecular mechanics and molecular dynamics simulations to ensure a global energy minimum at a given loading level. We have applied the present method to various carbon nanostructures including carbon nanotubes (CNTs), graphene, CNT with defects and CNT-graphene junctioned nanostructures. For all cases, we have identified the maximum stress and strain at failure of these carbon nanostructures as well as their critical failure modes, and discussed mechanisms that lead to their catastrophic failure.

1. Introduction

With increasing needs for better efficiency, more and more modern structural systems, satellites and space structures require multi-functionality having not only structural integrity but also thermal and electrical performance. Many previous studies have shown that carbon-based molecular structures such as diamond, carbon nanotube (CNT), and graphite, possess superior multifunctional properties including stiffness, strength, thermal and electrical conductivities because of their ordered structures as well as strong carbon-carbon (C-C) bonds. There are numerous efforts to enhance the performance of the composite structures and materials by taking advantage of these superior multi-functional properties of the carbon nanostructures.

CNTs and graphite are inherently 1-D and 2-D structures, and hence, their physical properties are highly anisotropic in nature. Recently, many efforts have been made to fabricate more advanced carbon nanomaterials by having 3-D junctioned structures with the CNTs and the graphene layers. One of such structures is a pillared graphene nanostructure (PGN), which can be fabricated by growing CNT forests on graphene/graphite layers. The 3-D carbon nanostructures have drawn much attention lately among researchers because of their superior multifunctional properties in 3-D directions, which are difficult to achieve with pure 1-D CNTs or 2-D graphene and graphite structures.

In order for these carbon nanostructures to be used as reinforcing constituents in the advanced composite materials and structures, one needs to assess their structural performance subject to various loading conditions. Such structural performance can be evaluated by mechanical properties such as stiffness, maximum stress and strain to failure, etc. Among numerical work to predict the mechanical properties of the carbon-based molecular architectures, widely and promisingly used are an atomistic modeling, such as molecular dynamic (MD) simulations [1, 2], tight binding MD [3], density functional theory [4], classical continuum mechanics [5-7] and structural mechanics approach [8, 9], etc. While many aspects of the carbon nanostructures have been discussed in literature, only a few studies have been conducted to predict their mechanical strength subject to various modes of loading such as tension, compression and shear loads, especially for the complicated 3-D carbon nanostructures.

In the current study, we have developed a computational method to predict the mechanical strength of various carbon nanostructures, such as CNTs, graphene sheets, CNT-graphene and CNT-CNT junctioned nanostructures, and have identified their critical failure modes. The details of the simulation methodology are summarized in the following section.

2. Simulation Methodology

The method used in the strength prediction of various carbon nanostructures is based on combined molecular mechanics (MM) and molecular dynamics (MD) simulation schemes. All the simulations were conducted with molecular simulation software, LAMMPS [10]. As will be discussed below, the MM and MD schemes ensure the realization of globally minimal energy configuration of the carbon nanostructures at a given loading and boundary conditions.

The strength prediction simulation starts with an initial configuration of a nanostructure by applying a small increment of the strain (typically 0.01~0.1% strain) in a desired loading direction. Other portions of carbon atoms are constrained by prescribed boundary conditions depending on modes of loading. The increment of the applied strain results in increase of an interatomic potential energy, while the kinetic energy remains unchanged under an assumption of static loading. We conducted the MM simulations to find the minimal energy configuration subject to increased interatomic potential at each loaded stage. General interatomic potentials of various carbon nanostructures based on sp^2 hybridized bonds and their potential parameters are obtained from [11, 12].

Since the molecules are to be loaded under static loading conditions, we only consider the potential energy and ignore the kinetic energy. Therefore, we have a single function of the potential energy to minimize with $3N$ independent variables, which are the 3 components of the coordinates (x, y and z) of N atoms in the system. When the set of atoms are loaded at the boundaries, the whole system of atoms is repositioned with the minimal energy configuration. We used a conjugate gradient method implemented in LAMMPS to find the equilibrium configuration of the atoms of the minimal energy. In conducting the MM simulations for searching the minimal energy configuration, the numerical scheme implemented in LAMMPS software does not guarantee the global minimum of the total potential energy states. Therefore, with complicated atomic structures, the MM scheme often leads to a local energy minimum configuration, which would adversely influence the damage initiation and subsequent progression resulting in unreliable prediction values. To circumvent this problem, we implemented an additional step to find the global energy configuration by

coupling the MM scheme with the MD simulations under an NVE (microcanonical) ensemble.

Under this ensemble, the MD simulations are conducted with constant number of atoms, simulation volume and total energy. The total energy consists of the potential energy and kinetic energy. During MM simulation stage, which is static simulation, the kinetic energy is zero since the velocities of the atoms are zero. In the local energy minimum configuration found by the MM simulations using LAMMPS, the force components as a whole atomic structure are zero, but the force components with respect to individual degrees of freedom of the atoms are not zero. During the MD simulation stage, accelerations and velocities of the atoms are calculated based on these non-zero force components acting on the atoms, which results in nonzero kinetic energy. Therefore, running the MD simulations effectively perturbs the system along the gradient directions by introducing the kinetic energy to the system. Since the NVE simulations ensure the total energy to remain constant, the increase in the kinetic energy results in reducing the potential energy by the same amount, which effectively results in jumping out of the local minimum and going down towards the global minimum direction. Therefore, by alternating the combined MM and MD simulations in an iterative way, we ensure to search the globally minimal energy state at a given loading step.

Upon finding equilibrium configuration at the given strain-loading stage, resulting stress components were obtained by calculating pressure components acting on the boundaries surrounding the carbon atoms. With the stress and strain components known, we obtained the stress-strain behavior of the carbon nanostructures with the load increase for various studied cases.

Figure 1 shows a flowchart that summarizes the present strength prediction scheme. Starting with the initial configuration of a nanostructure, a small increment of the strain is applied in a desired loading direction. While the increased strain is smaller than a preset maximum strain value, the MM simulation is conducted to find the minimal energy configuration using the Morse and other related potentials with respect to C-C bonds' deformation modes. Resulting stress and strain components are then calculated after the MM simulations. The system is then perturbed by the NVE MD simulations with a preset number of iterations. The combination of the MM and the MD simulations are repeated until the kinetic energy contribution to the total energy becomes negligibly small, and so do the force components acting on all atoms. We evaluate the amount of kinetic energy in terms of a temperature of the system, and used the system temperature as an exit criterion. If the system temperature is larger than a preset tolerance temperature, T_{tol}, the velocity components of all atoms are set to zero to suppress the kinetic energy contribution, and the MM simulations are conducted to obtain a new minimal energy state. When the system temperature is smaller than $T_{tol} = 10^{-6}$ K, we consider that the kinetic energy contribution to the total energy becomes negligibly small, and thus exit the current iteration loop of the MM and the MD combinational simulations for this loading step. After increasing the strain, the combination of the MM and MD simulations are repeated to search the global energy minimum configuration at this load step as discussed above.

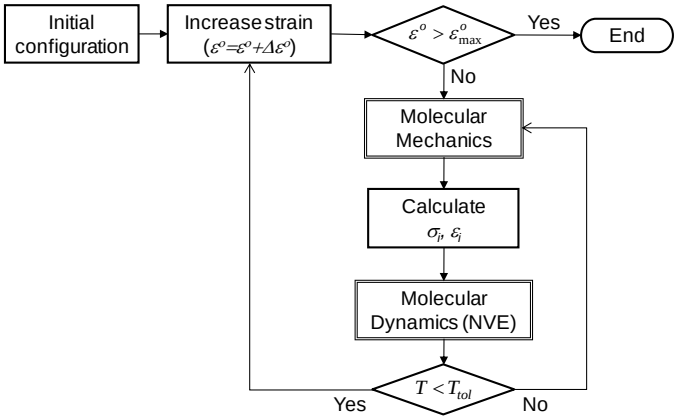

Figure 1. Strength prediction analysis scheme for carbon nanostructures.

3. Results and Discussions

We used the present method to predict the failure behavior and the stress-strain curves of various carbon nanostructures. The first case we considered is the graphene sheet under tensile loading in two in-plane directions (*x*- and *y*-directions) and horizontal shear loading. Stress-strain curves and deformed shapes at various strain states are plotted in Figure 2. Note that periodic boundary conditions are specified for each case. Note also that for visualization purpose, we plot the atom bonds with a cutoff distance of 0.16 nm, and therefore, any bonds greater than this cutoff distance are not drawn. As Figure 2(a)-(b) show, under the tensile loading, the graphene sheet stretches uniformly along the loading direction and the axial stress increases monotonically with the increase of the strain loading until it reaches a maximum stress level. The maximum stresses under the tensile loads in *x*- and *y*-directions are σ_1=95.7 GPa at ε_1=15.7% strain, and σ_2=120.3 GPa at ε_2=21.6%, respectively. While the graphene sheet stretched in *x*-direction shows a drastic stress drop right after the maximum stress, the graphene sheet stretched in *y*-direction continues to sustain the maximum stress level until the drastic stress drop at ε_1=22.2%. The main reason of the drastic stress drop is that the graphene sheet is unable to stretch uniformly along the loading directions, so that some C-C bonds are stretched more than other bonds to maintain the minimal energy state. For the loading in *x*-direction, the longer stretch of bonds occurs along a vertical line perpendicular to the loading direction, while for the loading in *y*-direction, the longer stretch occurs along a line perpendicular to the loading direction, but not in a straight way. For the shear load case, the stress increases monotonically with the increase of strain loading until at τ_{12}=154.0 GPa and ε_{12}=35.4%., and drops drastically with further increase of loading, as Figure 2(c) show.

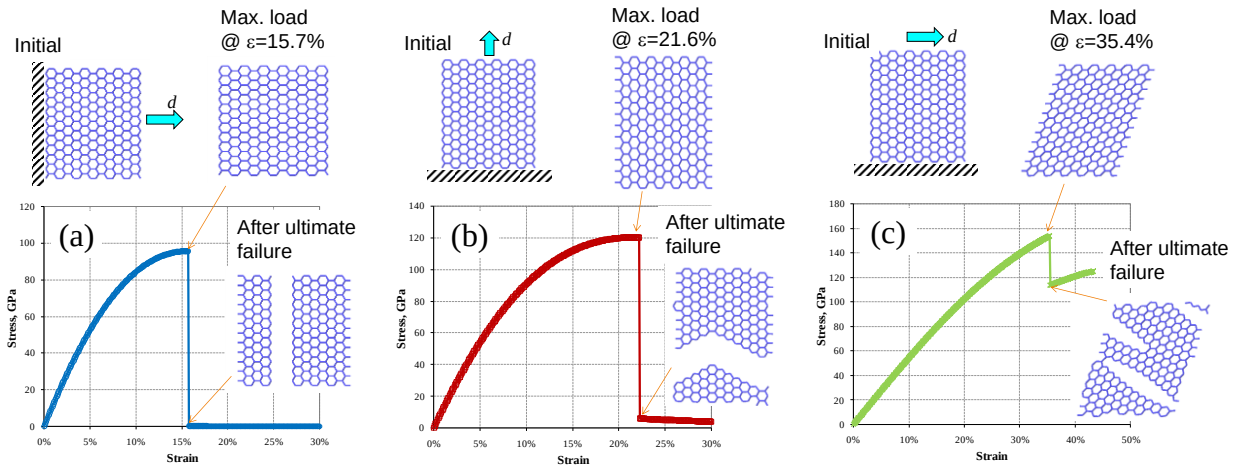

Figure 2. Graphene layer under (a) tensile loading in x-direction; (b) tensile loading in y-direction; (c) shear loading.

The next case considered is the CNTs under tensile and compressive loading. The results for four different chiralities of (6,0), (6,6), (12,0) and (12,12) CNTs are shown in Figure 3. The figure shows that zigzag (6,0) and (12,0) CNTs yields lower failure stress and strain than armchair (6,6) and (12,12) CNTs do. While the fractured surface of zigzag CNTs is nearly perpendicular to the loading direction, the fractured surface of the armchair CNTs has a slanted angle near 30º. For all CNTs, significant load drops occur after the catastrophic damage. When we compared the stress-strain curves of the graphene sheets and CNTs in Figure 2 and Figure 3, it can be seen that the stress-strain behaviors of the zigzag CNTs are similar with that of the graphene sheet loaded in *x*-direction, while those of the armchair CNTs are similar with that of the graphene sheet loaded in *y*-direction.

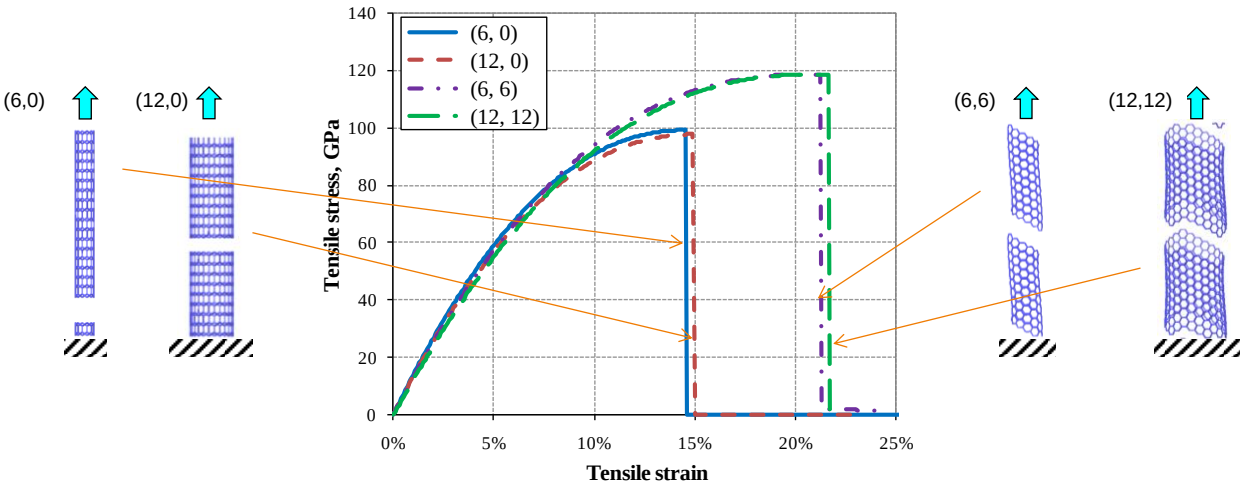

Figure 3. CNT with four different chiralities under uniaxial tensile loading.

We have applied the present method to predict the buckling behavior of the CNTs by applying the compressive loading along the CNT's length direction. Figure 4(a) shows the stress-strain curve and the deformed shapes of a (10,10) CNT with the length of 10 nm at various strain states under the compressive loading. The CNT is uniformly compressive in the axial direction until it starts to buckle to bend. As shown in the stress-strain curve, the CNT is compressed nearly linearly until the buckling at σ_1=123.0 GPa and ε_1=8.3%. With the further compression, the (10,10) CNT continues to buckling and forms hinges in two locations. .

Figure 4(b) shows the stress-strain curve and the deformed shapes of the same (10,10) CNT with a longer length of 30 nm. This longer CNT shows simpler Euler-type buckling shape. The stress-strain plots comparing the two CNTs of 10 nm and 30 nm long show that the maximum buckling stress is significantly dependent on the aspect ratio of the CNT, and the trend is that the maximum buckling stress decreases as the CNT length increases.

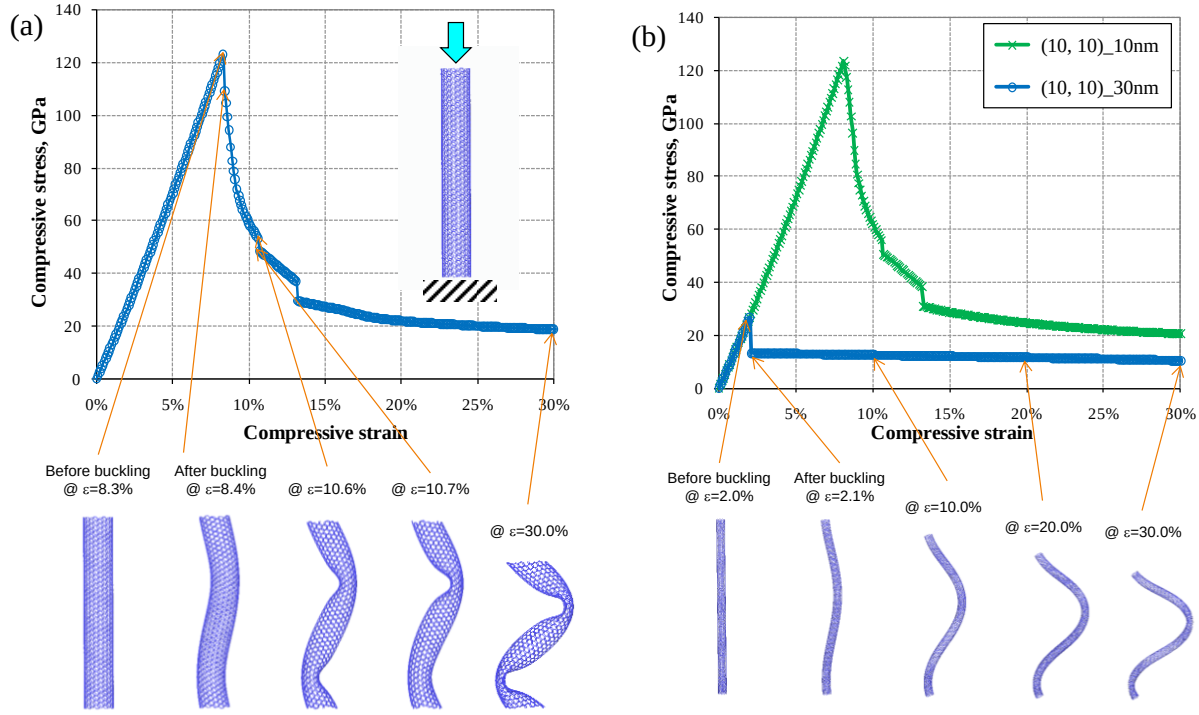

Figure 4. (10,10) CNTs under compressive loading: (a) 10 nm long and (b) 30 nm long CNTs.

Many CNTs fabricated in the labs tend to have many defects, which would affect the properties significantly. We have also applied the present method to evaluate the effects of defects on the mechanical properties (such as modulus and strength) of CNTs. A defected CNT was constructed with a semiconductor (8,0) and metallic (7,1) CNTs by fusing them at the junction, which forms a small-angle connection [13, 14]. Figure 5(a) shows the stress-strain curve and the deformed shapes of the (8,0)/(7,1) CNT at various strain states under the uniaxial tensile loading. To make smooth transition between the CNTs, the junction tends to form non-hexagonal C-C rings. In this (8,0)/(7,1) CNT case, the junction between these two CNTs consists of one pentagon and one heptagon C-C rings. As the deformed shapes show, the CNT junction with the defects initially flattens with the load increase until the fracture at the defected junction. It is clearly seen that the defected junction is the source of initiation of the damage, and results in the drastic stress drop. To evaluate the effect of defect on the mechanical properties, the stress-strain curve of the defected CNT are compared with those of pristine (8,0) and (7,1) CNTs, and replotted in Figure 5(b). The comparison plot shows that not only the initial slope (stiffness) but also the maximum fracture strength of the (8,0)/(7,1) CNT are significantly lowered because of the defected junction. This simulation result supports the observation that why the experimentally measured stiffness and strength values of CNTs are significantly lowered than theoretically predicted values since the most CNTs fabricated in reality possess many defects.

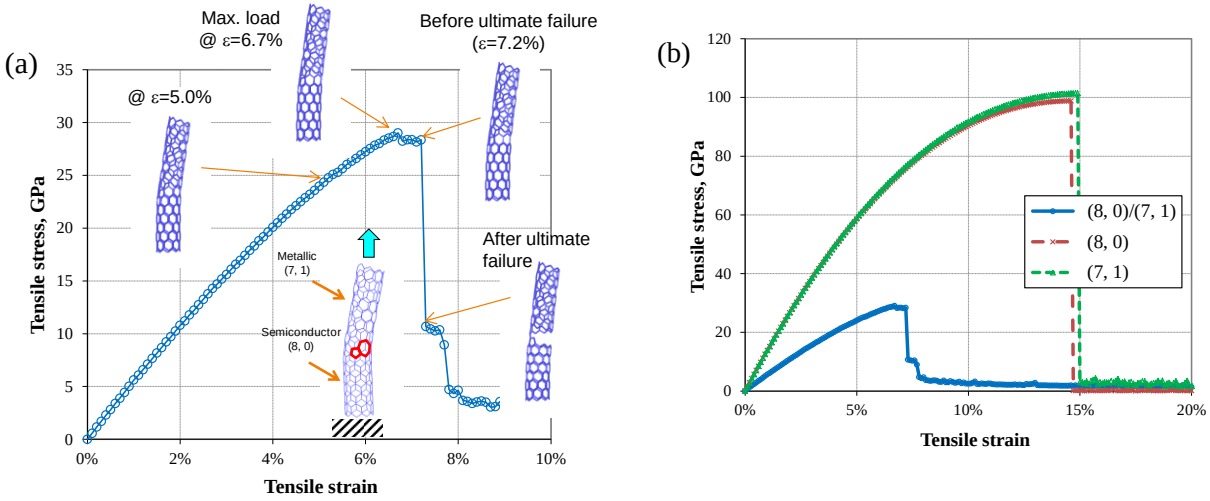

Figure 5. (a) A CNT with a defected junction under tensile loading; (b) Comparison of the stress-strain plots of the defected (8,0)/(7,1) CNT and pristine (8,0) and (7,1) CNTs.

The junction between the CNT and graphene in the 3-D junctioned PGN consists of several non-hexagonal C-C rings. As in the case of the defected CNT, the non-hexagonal C-C rings tend to be the source of initiation of the damage and may result in the drastic stress drop. Furthermore, because of column nature structures, it is susceptible to buckling damage subject to compressive loading. We take a representative unitcell of such 3-D CNT-graphene junctioned nanostructure, and evaluate their structural performance under tensile and compressive loading. Figure 6 shows the stress-strain curves of single-walled CNT grown on graphene sheet under tension and compression loading. The stress-strain plot shows that the initial slopes for the tension and compression are similar with other. However, these two modes of loading results in drastically different maximum strength values as well as post-failure behaviors. Note that the failure occurs near the CNT-graphene junctions in both cases because of the heptagonal rings around the junction. Note also that after this junctioned nanostructure buckles under the compression, the stress-strain curve becomes flattened, which is similar to a post-failure densification behavior of porous foam materials.

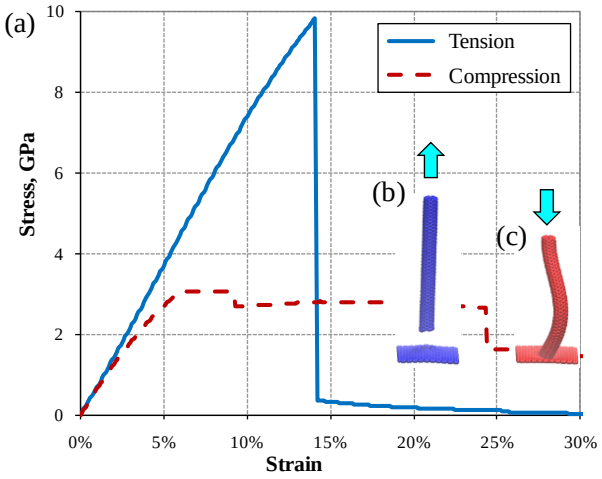

Figure 6. A CNT-graphene junctioned 3-D carbon nanostructure under tensile and compressive loading.

4. Summary and Conclusions

We have developed the computational scheme to predict stiffness and strength of carbon nanostructures under various loading modes. The prediction method is based on combined MM and MD simulations by ensuring the global energy minimum at a given loading level. The MM simulations enable us to conduct the simulations with reasonably large load increment, while the MD simulations help us in finding the global energy minimum at each load step. We have applied the present method to various carbon nanostructures including 1-D CNTs, 2-D graphene, CNT with defects and 3-D CNT-graphene junctioned carbon nanostructures. We have identified the maximum stress and strain at failure of these carbon nanostructures as well as their critical failure modes.

5. Acknowledgments

This work was performed under U.S. Air Force Contract No. FA8650-10-D-5011 and Air Force Office of Scientific Research.

References

[1] S. Iijima, C. Brabec, A. Maiti and J. Bernholc. Structural flexibility of carbon nanotubes. *The Journal of Chemical Physics*, 104(5):2089-2092, 1996.

[2] B. I. Yakobson, M. P. Campbell, C. J. Brabec and J. Bernholc. High strain rate fracture and C-chain unraveling in carbon nanotubes. *Computational Materials Science*, 8(4):341-348, 1997.

[3] E. Hernández, C. Goze, P. Bernier and A. Rubio. Elastic Properties of C and BxCyNz Composite Nanotubes. *Physical Review Letters*, 80(20):4502-4505, 1998.

[4] D. Sánchez-Portal, E. Artacho, J. M. Soler, A. Rubio and P. Ordej. Ab initio structural, elastic, and vibrational properties of carbon nanotubes. *Physical Review B*, 59(19):12678-12688, 1999.

[5] C. Q. Ru. Effective bending stiffness of carbon nanotubes. *Physical Review B*, 62(15):9973-9976, 2000.

[6] C. Q. Ru. Elastic buckling of single-walled carbon nanotube ropes under high pressure. *Physical Review B*, 62(15):10405-10408, 2000.

[7] Y. J. Liu and X. L. Chen. Evaluations of the effective material properties of carbon nanotube-based composites using a nanoscale representative volume element. *Mechanics of Materials*, 35(1-2):69-81, 2003.

[8] C. Li and T.-W. Chou. A structural mechanics approach for the analysis of carbon nanotubes. *International Journal of Solids and Structures*, 40(10):2487-2499, 2003.

[9] C. Li and T.-W. Chou. Elastic moduli of multi-walled carbon nanotubes and the effect of van der Waals forces. *Composites Science and Technology*, 63(11):1517-1524, 2003.

[10] S. Plimpton. Fast Parallel Algorithms for Short-Range Molecular Dynamics. *Journal of Computational Physics*, 117(1):1-19, 1995.

[11] T. Belytschko, S. P. Xiao, G. C. Schatz and R. S. Ruoff. Atomistic simulations of nanotube fracture. *Physical Review B*, 65(23):235430, 2002.

[12] H. Sun, S. J. Mumby, J. R. Maple and A. T. Hagler. An ab Initio CFF93 All-Atom Force Field for Polycarbonates. *Journal of the American Chemical Society*, 116(7):2978-2987, 1994.

[13] L. Chico, V. H. Crespi, L. X. Benedict, S. G. Louie and M. L. Cohen. Pure Carbon Nanoscale Devices: Nanotube Heterojunctions. *Physical Review Letters*, 76(6):971-974, 1996.

[14] V. Meunier, L. Henrard and P. Lambin. Energetics of bent carbon nanotubes. *Physical Review B*, 57(4):2586-2591, 1998.